ACS central science

Research Article

http://pubs.acs.org/journal/acscii

Stereoisomerism in Nanohoops with Heterogeneous Biaryl Linkages of *E/Z*- and *R/S*-Geometries

Parantap Sarkar,[†] Zhe Sun,[†,‡] Toshiki Tokuhira,[§] Motoko Kotani,[†,#] Sota Sato,[†,‡] and Hiroyuki Isobe*[,†,‡,§]

[†]Advanced Institute for Materials Research, Tohoku University, Aoba-ku, Sendai 980-8577, Japan

[‡]JST, ERATO, Isobe Degenerate π-Integration Project, Aoba-ku, Sendai 980-8577, Japan

[§]Department of Chemistry, The University of Tokyo, Hongo, Bunkyo-ku, Tokyo 113-0033, Japan

[#]Mathematical Institute, Tohoku University, Aoba-ku, Sendai 980-8578, Japan

Supporting Information

ABSTRACT: The stereochemistry of cycloarylene nanohoops gives rise to unique cyclostereoisomerism originating from hoop-shaped molecular shapes. However, cyclostereoisomerism has not been well understood despite the ever-increasing number of structural variants. The present work clarifies the cyclostereoisomerism of a cyclophenanthrenylene nanohoop possessing both *E/Z*- and *R/S*-geometries at the biaryl linkages. Involvement of the *R/S* axial chirality in the nanohoop leads to the deviation of the structure from a coplanar belt shape and allows for structural variations with 51 stereoisomers with *E/Z*- and *R/S*-geometries. Experimental investigations of the dynamic behaviors of the cyclophenanthrenylene nanohoop revealed the presence of two-stage isomerization processes taking place separately at the *E/Z*- and *R/S*-linkages. Consequently, despite the presence of *E/Z*-fluctuations, the *R/S* axial chirality resulted in a separable pair of enantiomers. The structural information reported here, such as geometric descriptors and anomalous dynamics, may shed light on the common structures of various nanohoops.

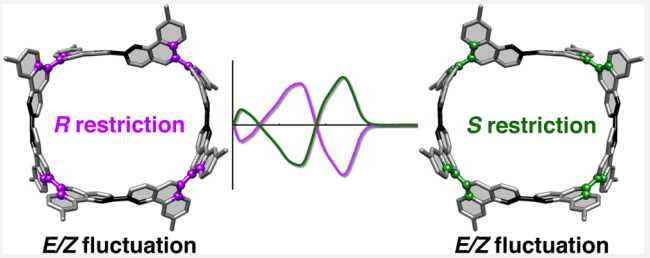

INTRODUCTION

Pervading all of chemistry, stereochemistry is an indispensable concept in any field allied with the central science of molecules.[1] When embedded in cyclic molecules, the stereochemistry results in an interesting stereoisomerism (cyclostereoisomerism) accompanying isomer degeneracies.[1−3] The cyclostereoisomerism also emerges in hoop-shaped, sp^2-carbon networks of cycloarylenes, called nanohoops,[4−7] and gives rise to unique planar chirality in the persistent belt-shaped structures mimicking single-wall carbon nanotubes (SWNT).[8,9] For instance, stereoisomers of cycloarylenes with persistent belt shapes such as [4]cyclo-2,8-chrysenylene ([4]$CC_{2,8}$), [4]cyclo-3,9-chrysenylene ([4]$CC_{3,9}$), and [4]-cyclo-2,8-anthanthrenylene ([4]$CA_{2,8}$) have been isolated and identified (Figure 1),[10−13] and the belt-shaped enantiomers have been distinguished by *P/M* descriptors of SWNTs.[8,14] The isolation and identification confirmed the presence of curved, coplanar arrays of arylene panels for the first time, and the coplanar arrays formed and defined a cylindrical surface around the center axis. The shape of these molecules is best described, from a geometric, mathematical point of view,[15,16] as a cylinder, and therefore, the original description of the cylindrical structure of SWNT, "roll of the hexagonal (graphitic) sheet about the filament axis",[17] becomes applicable to the molecular entities. Taking account of the relevant facts, we used the term belt/tube to describe these molecular shapes and named these first examples as belt-persistent cycloarylenes/nanohoops or finite SWNT molecules.[18] More recently, the cyclostereoisomerism of belt-shaped cycloarylenes was further elucidated by structural investigations of a series of [*n*]cyclo-*amphi*-naphthylenes ([*n*]CaNAP; *n* = 6−11), and the structural degeneracies and the dynamic cyclostereoisomerism were revealed by mathematical and chemical methods.[19,20] The dynamic cyclostereoisomerism of [*n*]CaNAP further allowed us to draw a line between a persistent cylindrical shape and a fluctuating hoop shape. Thus, in the case of [*n*]CaNAP, [6]CaNAP spectroscopically possessed the persistent, cylinder/tube/belt shape, whereas [*n*]CaNAP with $n \geq 7$ possessed fluctuating shapes via rapid arylene rotations and lacked coplanar arylene arrays to define the cylinder/tube/belt.

In the belt-shaped nanohoops, the restricted biaryl rotations originated from macrocyclic ring strains to result in anomalous atropisomerism:[10−13,19,20] in the absence of steric repulsions, the biaryl linkages possessing 2,2′-binaphthyl structures in [6]CaNAP have been constrained at the coplanar, *E/Z* geometries. Conventionally, however, atropisomerism of biaryls such as 1,1′-binaphthyl was generated by steric repulsions between *ortho*-substituents, and the chirality emerged from the non-coplanar,*R/S* biaryl geometries.[1,2] Therefore, both of the

Received: August 20, 2016
Published: September 15, 2016

DOI: 10.1021/acscentsci.6b00240
ACS Cent. Sci. 2016, 2, 740−747

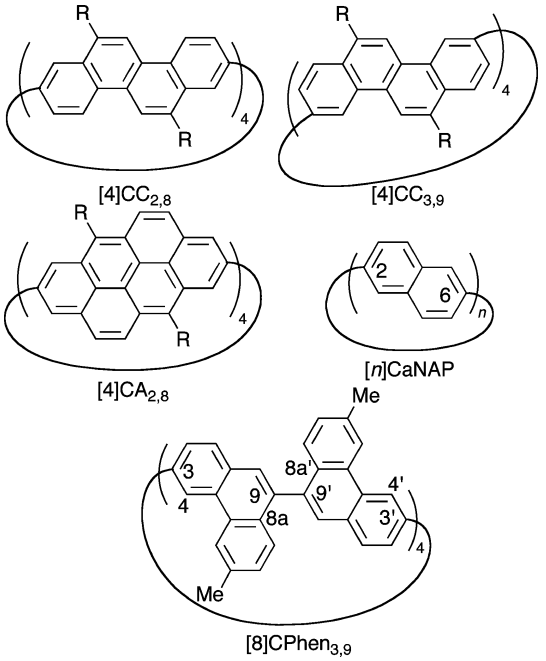

Figure 1. Structures of [8]CPhen$_{3,9}$ and relevant congeners.

constrained linkages, i.e., *E/Z* and *R/S* biaryl linkages, could give rise to the cyclostereoisomerism of nanohoops, but such heterogeneous cyclostereoisomerism originating from *E/Z* and *R/S* biaryl linkages has not been devised.[21−23] In this study, we explore the heterogeneous cyclostereoisomerism through the synthesis of [8]cyclo-3,9-phenanthrenylene ([8]CPhen$_{3,9}$) possessing different biaryl linkages at 3,3′- and 9,9′-connections. The 3,3′-linkage mimics the biaryl linkage of 2,2′-binaphthyl, and the 9,9′-linkage mimics the biaryl linkage of 1,1′-binaphthyl. With this nanohoop, enantiomers were separated despite the presence of structural fluctuations at the *E/Z* linkages. This result showed that the chirality in the non-belt-shaped arylene macrocycle originated from the intrinsic axial chirality at the constrained *R/S* linkages, which is in stark contrast to the unique chirality of belt-persistent congeners devoid of the axial chirality.[10,11,19,20] The cyclostereoisomerism reported in this study should be taken into account to understand and describe the common structures of non-belt-shaped nanohoop variants.

RESULTS AND DISCUSSION

Synthesis. We synthesized [8]CPhen$_{3,9}$ through a combination of several transformations. The stilbene **1**, synthesized via Perkin condensation,[24] was subjected to iodine-mediated, photochemical cyclization[25] to afford the phenanthrene derivative **2**. Photochemical conversion of carboxylic acid to iodide with 1,3-diiodo-5,5-dimethylhydantoin was found to be applicable with **2** for the synthesis of 9-iodophenanthrene derivative **3**. After unsuccessful attempts to use Ullmann coupling under several conditions, we found that a low-temperature condition in the presence of nitrobenzene[26] allowed for the site-selective coupling reaction to give 9,9′-biphenanthrenyl derivative **4**. After 9,9′-biphenanthrenyl was furnished with boryl moieties via Miyaura borylation,[27] Pt-mediated macrocyclization and subsequent reductive elimination[10] were performed to afford [8]CPhen$_{3,9}$.

Crystal Structure. We obtained a single crystal of [8]CPhen$_{3,9}$ and performed X-ray crystallographic analysis.

Scheme 1. Synthesis of [8]CPhen$_{3,9}$

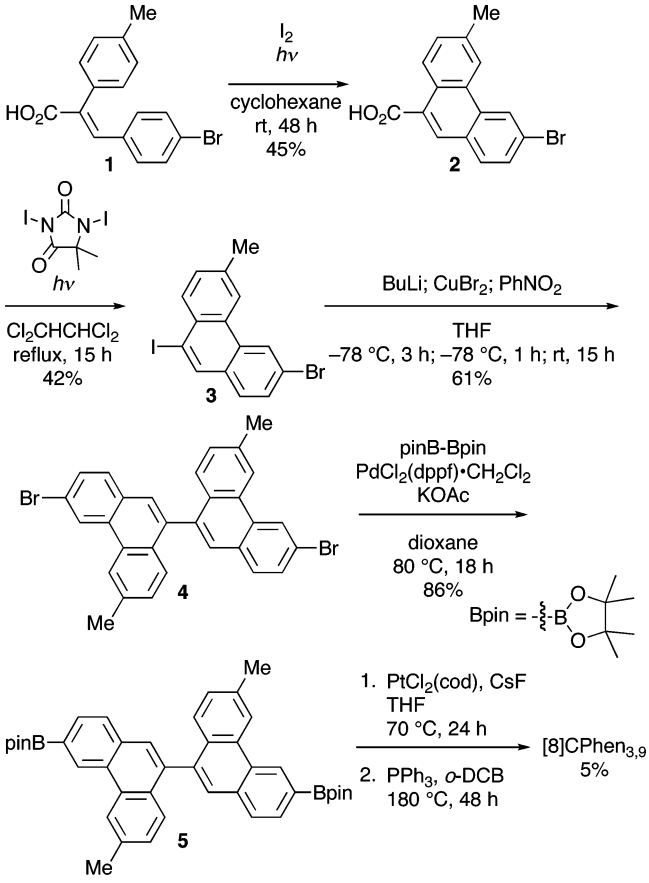

The crystal structure existed as a racemate, and two enantiomeric structures were determined. The dihedral angles measured with 4-3-3′-4′ carbon atoms at the 3,3′-linkages of the (*E,R,E,R,E,R,E,R*)-structure in Figure 2 were 141°, 149°,

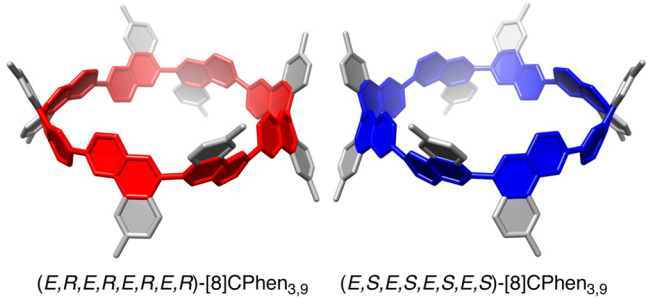

Figure 2. Crystal structures of [8]CPhen$_{3,9}$. An enantiomer pair found in the crystal is shown. Naphthylene units identical to those of [8]CaNAP are shown in red and blue (see ref 20). A minor structural deviation of one phenanthrenylene panel was found as a disordered structure, and the major structure with 83% occupancy was adopted as the representative structure for discussion.

166°, and 166°, and those with 8a-9-9′-8a′ atoms at the 9,9′-linkages were −142°, −142°, −143°, and −143° (see below for the descriptors and Figure 1 for the atom numbers). Thus, deviations from the coplanar biaryl orientations were 25° at the 3,3′-linkages and 38° at the 9,9′-linkages on average.

Possible Structures. We now describe the fundamental and possible structures, i.e., cyclostereoisomerism, of [8]-CPhen$_{3,9}$. The geometries of [8]CPhen$_{3,9}$ at the 3,3′- and 9,9′-

DOI: 10.1021/acscentsci.6b00240
ACS Cent. Sci. 2016, 2, 740−747

linkages share common biaryl linkages with 2,2′- and 1,1′-binaphthyl, respectively, and the intrinsic geometrical features of binaphthyls are described as structural references in the absence of macrocyclic structures. The geometry of the biaryl linkage of 2,2′-binaphthyl can be expressed using either the *E*/*Z* or *R*/*S* descriptors as shown in Figure 3.[1,2] However, the energy

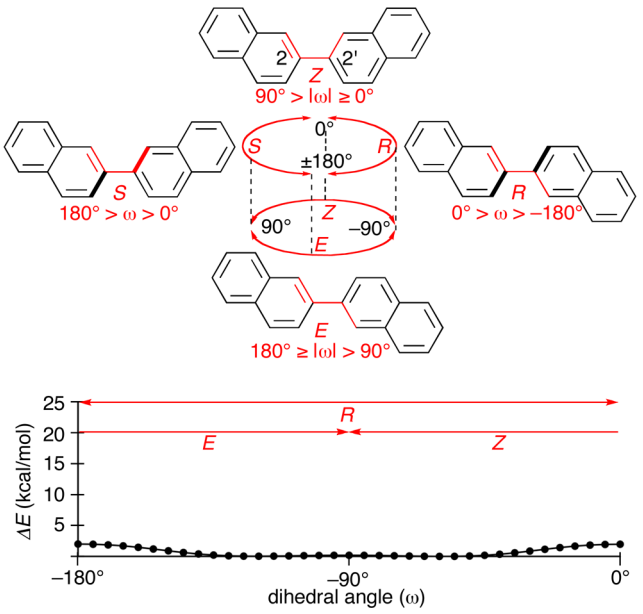

Figure 3. Structural features of 2,2′-binaphthyl. Two descriptors, *R*/*S* and *E*/*Z*, can describe the geometry at the biaryl linkage. The energy diagram for the biaryl rotation was obtained by the scan calculations between $\omega = -180°$ and 0° in +5° increments at the semiempirical PM6 level of theory.

barriers at both transitions ($\omega = \pm 90°$ or $0°/\pm 180°$) are low (<2 kcal/mol) and allow for free rotations at the linkages. The two geometrical descriptors of *E*/*Z* and *R*/*S* are, therefore, unnecessary or inappropriate for the description of the geometry at this biaryl linkage.[1,2]

The geometry of the biaryl linkage of 1,1′-binaphthyl can also be expressed using either the *R*/*S* or *E*/*Z* descriptors as shown in Figure 4. At this linkage, on the other hand, the energy barrier at *R*/*S* transitions becomes substantially high (+20 kcal/mol) and divides *R*- and *S*-geometries as two distinct species. This barrier at the *R*/*S* transitions is experimentally confirmed by the separation of enantiomers (see also below).[28−30] Hence, the descriptors of biaryl linkages are appropriately selected by considering the energy profiles of the biaryl rotations. In the case of 1,1′-binaphthyl, for instance, we should select one of the *R*/*S* descriptors and describe the specific geometry situated in the low-energy valley between two energy barriers at the *R*/*S* transitions.[1,2]

Geometric features of [8]CPhen$_{3,9}$ were elucidated by the theoretical calculations with the semiempirical PM6 method.[11,13] Scan calculations estimated the dihedral angles of the (*E*,*R*,*E*,*R*,*E*,*R*,*E*,*R*)-structure at the global minimum as 146° and −111° for the 3,3′- and 9,9′-biaryl linkages, respectively, and located the two energy barriers in the range of 180° (Figure 5). For the 3,3′-linkage, the low-energy valley spanned between the barriers at $\omega = 66°$ and −114°. Lacking barriers around $\omega = 180°$ of the *R*/*S* transition, the energy profiles confirmed the appropriateness of the *E* descriptor for this linkage.[31] For the 9,9′-linkage, the energy profile showed the absence of barriers

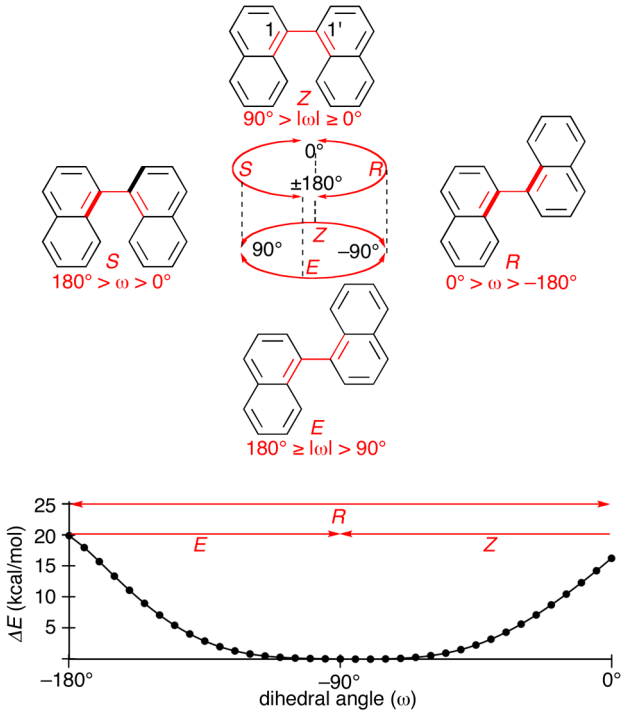

Figure 4. Structural features of 1,1′-binaphthyl. Two descriptors, *R*/*S* and *E*/*Z*, can describe the geometry at the biaryl linkage, and the energy diagram confirms the appropriateness of *R*/*S* descriptors. The energy diagram for the biaryl rotation was obtained by the scan calculations between $\omega = -180°$ and 0° in +5° increments at the semiempirical PM6 level of theory.

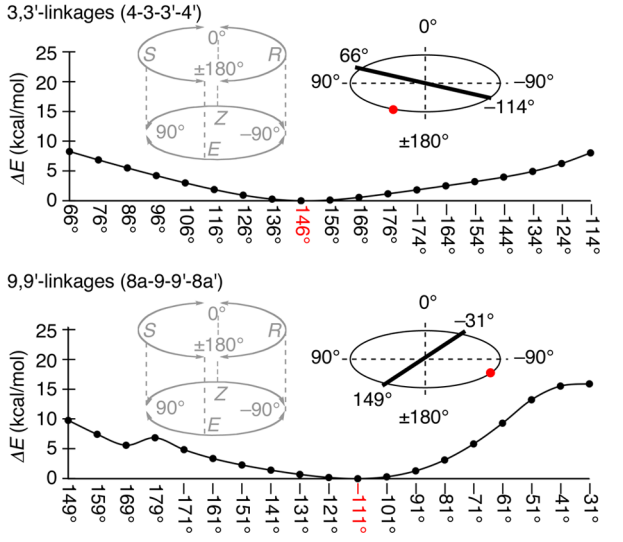

Figure 5. Energy profiles of the biaryl rotation in [8]CPhen$_{3,9}$ from scan calculations at the semiempirical PM6 level of theory. The dihedral angle was scanned for 180° rotations in ±10° increments.

for the *E*/*Z* transition around $\omega = -90°$, which suggested the *R* descriptor as the appropriate descriptor. These energy barriers for the biaryl rotations were further revealed by the experiments (see below).[32]

The presence of the *R*/*S* biaryl linkages in [8]CPhen$_{3,9}$ altered the cyclostereoisomerism from that of structurally relevant, *E*/*Z*-linked [8]CaNAP nanohoops. In the case of [8]CaNAP, the coplanar belt shape resulted in 30 stereoisomers comprising 18 diastereomers and 12 enantiomer pairs,

DOI: 10.1021/acscentsci.6b00240
ACS Cent. Sci. 2016, 2, 740−747

and the number of isomers was also obtained from mathematical equations.[20] However, the *R/S* linkages deviate the belt shape, and the non-belt shape containing axial chirality gives rise to a larger number of stereoisomers: there are 144 possible combinations of the *E/Z* and *R/S* linkages in [8]CPhen$_{3,9}$ structures, which results in 51 stereoisomers comprising 31 diastereomers and 20 enantiomer pairs (Table S1). We performed the density functional theory (DFT) calculations of all diasteroisomeric structures of [8]CPhen$_{3,9}$, and the (*E*,*R*,*E*,*R*,*E*,*R*,*E*,*R*)/(*E*,*S*,*E*,*S*,*E*,*S*,*E*,*S*)-enantiomers in crystal structures were found at the global minimum among 31 diastereomers. The energy differences of other diastereomers from the global minimum were less than +25 kcal/mol (Figure 6).

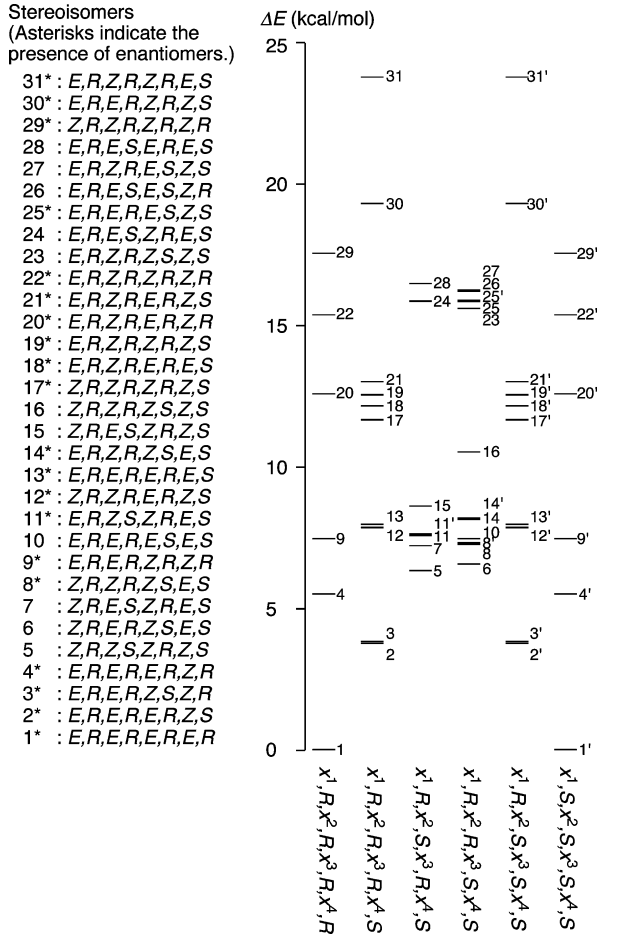

Figure 6. Stereoisomers and energetics of [8]CPhen$_{3,9}$. The energy diagram was obtained by calculations at the B3LYP/6-31G(d,p) level of theory.

Variable-Temperature NMR. The dynamics of the [8]CPhen$_{3,9}$ structure were experimentally investigated by variable-temperature (VT) NMR analysis. The ^{1}H NMR resonances comprising three singlets and four doublets corresponded to a set of resonances that can be assigned to a single phenanthrenylene panel (singlets = H^4/H^5/H^{10}, doublets = H^8/H^7/H^2/H^1) and were fully assigned with the aid of NOESY and COSY spectra (Figure S1, S2). This observation showed that, as a time-averaged structure, the most stable isomeric structure described by (*E*,*R*,*E*,*R*,*E*,*R*,*E*,*R*)/(*E*,*S*,*E*,*S*,*E*,*S*,*E*,*S*) with the D_4 point symmetry was observed.

The aromatic regions of the VT NMR spectra in the temperature range of 80 °C to −90 °C are shown in Figure 7a.

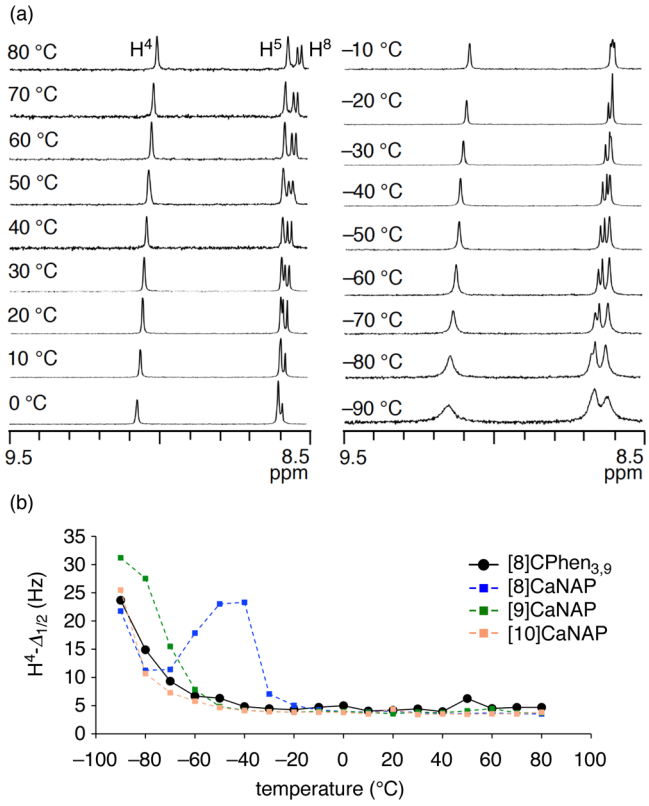

Figure 7. VT NMR analysis of [8]CPhen$_{3,9}$. (a) Spectra of the aromatic region showing representative ^{1}H resonances in toluene-d_8. See Figure S3 for the whole aromatic region. (b) Temperature dependence of full width at half-maximum ($\Delta_{1/2}$) of the H^4 resonance. Reference data of [*n*]CaNAP (*n* = 8−10) were taken from ref 20.

As was the case with [*n*]CaNAP, the diastereomers as well as the resonance splitting were not observed during the VT measurement, but the analysis of broadening-resharpening behaviors provided information about the dynamics.[20,33−35] Thus, a singlet proton resonance at the 4-position (H^4) appeared separately in the low-field region (~9 ppm) and was suitable for the broadening-resharpening analysis. The temperature dependence of the full width at half-maximum of the H^4 resonance (H^4-$\Delta_{1/2}$) is summarized in Figure 7b together with the reference data of [*n*]CaNAP (*n* = 8−10). Thus, the H^4 resonance showed two-stage broadening-resharpening behaviors: the sharp singlet peak at 80 °C was broadened upon cooling to 50 °C, sharpened upon further cooling to 40 °C, and broadened again toward −90 °C. The two-stage behavior showed the presence of two transitions in the dynamic isomerization of [8]CPhen$_{3,9}$. The high-temperature transition with the temperature peak at 50 °C could potentially be used for the kinetic analysis of the dynamics.[20] However, the population of the hidden, exchanging partners at this temperature was estimated as ca. 50% in comparison with the sharp peak at 40 °C and was too high for reliable analysis.[33−35]

Qualitative yet important information was obtained from the low-temperature transition. As shown in Figure 7b, the $\Delta_{1/2}$ value was increased toward −90 °C to give a temperature-dependent curve similar to that of [10]CaNAP. Considering that the $\Delta_{1/2}$ value depends on the rate constant of

DOI: 10.1021/acscentsci.6b00240
ACS Cent. Sci. 2016, 2, 740−747

isomerization among the diastereomeric structures,[20,33,34] we may conclude that the dynamic characteristics of the low-temperature isomerizations of [8]CPhen$_{3,9}$ and [10]CaNAP are similar. Because the fundamental structure of [8]CPhen$_{3,9}$ at the 3,3′-linkages is identical to biaryl linkages of [10]CaNAP, we conclude that the common *E*/*Z* isomerization at this site is the origin of the low-temperature transition. The high-temperature transition of [8]CPhen$_{3,9}$ should therefore be ascribed to the *R*/*S* isomerization at the 9,9′-linkages, as was further supported by the analysis using the VT CD spectra (see below).

Separation of Enantiomers. Albeit unexpectedly, we succeeded in separating the enantiomers of [8]CPhen$_{3,9}$. When we analyzed [8]CPhen$_{3,9}$ with HPLC using cholesterol-loaded silica gel columns (COSMOSIL Cholester),[10] two compounds with opposite CD signals were detected (Figure 8a).[36] After isolation of two isomers on a preparative scale

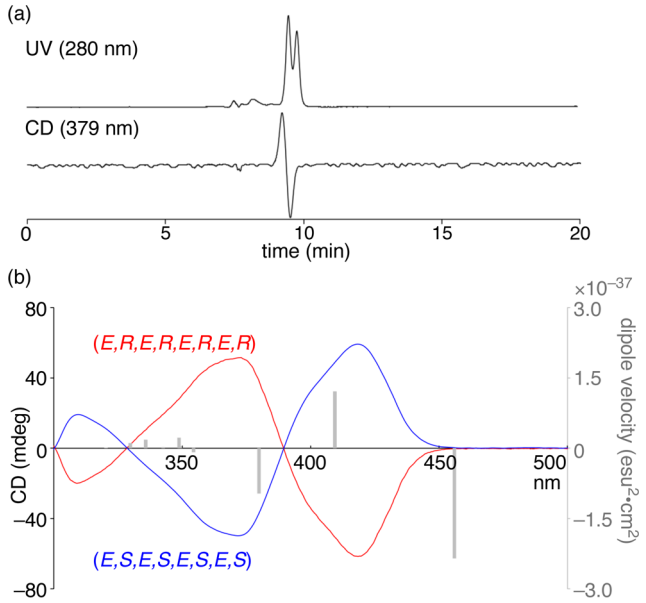

Figure 8. Isolation and CD spectra of [8]CPhen$_{3,9}$ enantiomers. (a) Analytical HPLC chromatogram of [8]CPhen$_{3,9}$. Conditions: column = COSMOSIL Cholester (4.6ϕ, 250 + 250 + 250 mm), eluent = 30% methanol in chloroform. (b) CD spectra of isolated enantiomers in toluene at 25 °C. Gray bars show the rotatory velocity calculated by the DFT method at the B3LYP/6-31G(d,p) level of theory for the (*E*,*R*,*E*,*R*,*E*,*R*,*E*,*R*)-structure.

(Figures S4 and S5), the analysis with CD spectroscopy showed mirror-image spectra to confirm their enantiomeric relationship (Figure 8b). To elucidate the absolute configurations, we calculated the theoretical rotatory velocity of the (*E*,*R*,*E*,*R*,*E*,*R*,-*E*,*R*)-structure with the time-dependent DFT method at the B3LYP/6-31G(d,p) level of theory (Figure 8b). Comparison of the theoretical signals with the experimental spectra required careful considerations for the following reasons. First, spectral analysis with the B3LYP functional tends to underestimate the excitation energy.[37] For instance, the theoretical spectrum of belt-shaped [4]CC$_{2,8}$ was red-shifted by ca. 15 nm.[10,38,39] Second, the NMR spectra showed the presence of isomerization processes among the diastereomers at 25 °C (see above), which should also result in shortening of the conjugation in the real systems and thus in the theoretical underestimation of the excitation energy from one conformer.[40] Therefore, these two factors should commonly result in a red-shifted theoretical spectrum, so that the ordering of the states between the experimental and theoretical spectra should be examined with these considerations in mind. Thus, the major theoretical CD signals from the low to high energy regions (red-to-blue order) predict negative, positive, and negative signals for the (*E*,*R*,*E*,*R*,*E*,*R*,*E*,*R*)-structure, and we assigned this isomer as the time-averaged structure for the experimental CD spectrum shown in red in Figure 8b.[41]

Variable-Temperature CD. Isolation of enantiomers allowed us to investigate racemization kinetics using the VT CD spectra. As a reference, we first performed the racemization analysis of an enantiomer of 9,9′-phenanthrenyl, (−)-**4**.[42] According to the methods established for biaryls,[28−30] the racemization process was followed by the decay of the maximum CD signal at 302 nm for the 30−60 °C temperature range (Figures S6−S9). Representative data at 30 °C are shown in Figure 9a. The racemization proceeded as the first-order

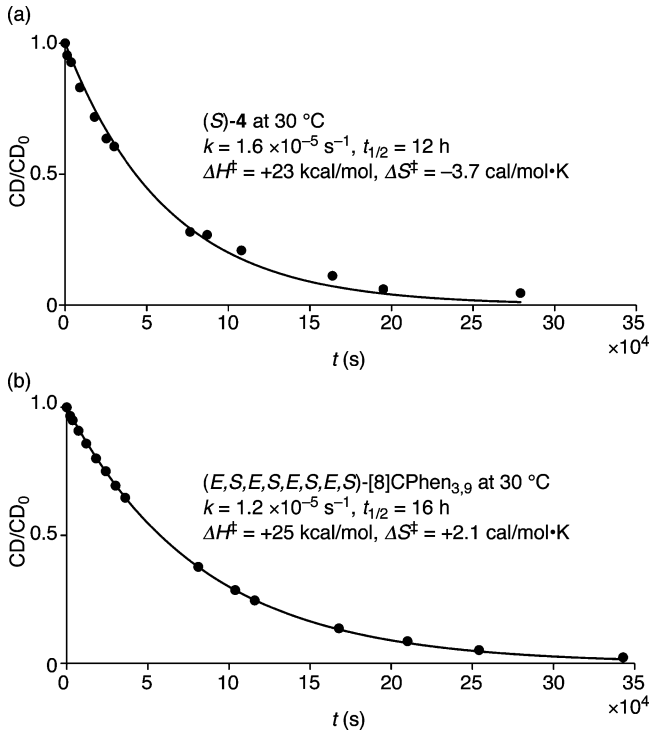

Figure 9. Racemization kinetics. (a) Racemization of (−)-**4** at 30 °C followed at 302 nm. The coefficient of determination (R^2) was 0.994199021 and confirmed the sufficient goodness of fit for the analysis. (b) Racemization of (*E*,*S*,*E*,*S*,*E*,*S*,*E*,*S*)-[8]CPhen$_{3,9}$ at 30 °C followed at 419 nm. The coefficient of determination (R^2) was 0.999784569 and confirmed the sufficient goodness of fit for the analysis.

reaction and by fitting the racemization curves to $k = t^{-1} \cdot \ln(CD_0/CD)$,[28,29] the rate constant and half-life were estimated as $k = 1.6 \times 10^{-5}$ s^{-1} and $t_{1/2}$ = 12 h at 30 °C, respectively.[29,43] The temperature-dependence of the rate constant was analyzed using the Eyring equation to obtain the energy barriers of $\Delta H^{‡}$ = +23 kcal/mol and $\Delta S^{‡}$ = −3.7 cal/mol·K (Figure S10). As expected, the energetics of the racemization were similar to those observed with 1,1′-binaphthyl ($\Delta H^{‡}$ = +22 kcal/mol, $\Delta S^{‡}$ = −5.2 cal/mol·K).[44] For both cases, the enthalpy term was the major contributor to the energy barrier.

DOI: 10.1021/acscentsci.6b00240
ACS Cent. Sci. 2016, 2, 740−747

Using the same method, we then analyzed the racemization of isolated (*E,S,E,S,E,S,E,S*)-[8]CPhen$_{3,9}$. Thus, the decay of the maximum CD signal at 419 nm was tracked for the 30−60 °C temperature range. As shown in Figure 9b, the CD signal decreased exponentially with time and allowed the analysis using the first-order kinetics to obtain the rate constant k = 1.2 × 10^{-5} s^{-1} (30 °C), the half-life $t_{1/2}$ = 16 h (30 °C), and the energy barriers $\Delta H^{\ddagger}$ = +25 kcal/mol and $\Delta S^{\ddagger}$ = +2.1 cal/mol·K (Figures S11−S15). The enthalpy term played the dominant role in the energy barrier and was nearly identical to the value obtained for the racemization of (−)-**4** ($\Delta H^{\ddagger}$ = +23 kcal/mol).[45] This similarity suggested that, despite the presence of multiple *R/S* linkages, the macrocyclic structure exerted negligible effects on the energetics of racemization. Hence, *R/S* isomerization at the 9,9′-linkages served as the rate-determining steps for the racemization of [8]CPhen$_{3,9}$.

Isomerization Profiles. Combining the insights obtained from the DFT, VT NMR, and VT CD analyses, we may propose a plausible scenario for the isomerization processes of [8]CPhen$_{3,9}$. The DFT energies of stereoisomers (Δ*E*, Figure 6) emerging from the *R/S* and *E/Z* geometries are summarized in two-dimensional profiles shown in Figures 10 and S16.[46,47]

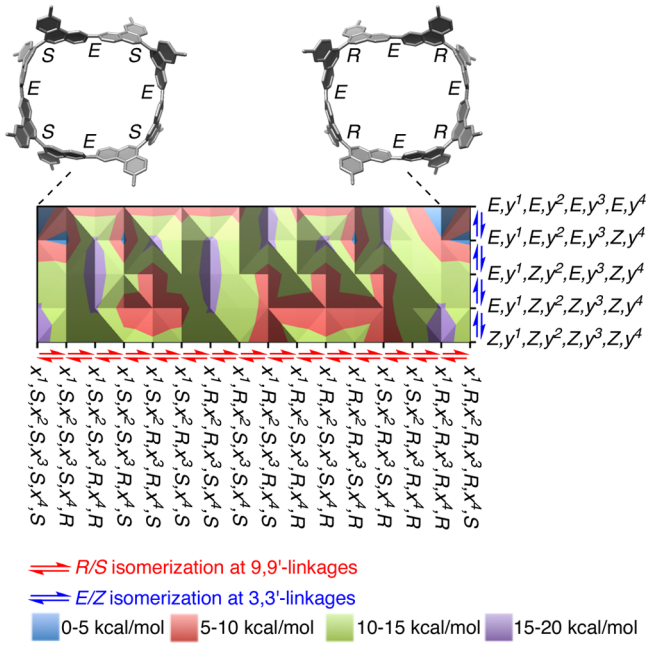

Figure 10. Isomerization profile of [8]CPhen$_{3,9}$. Adjacent isomers are interconvertible through a single-linkage rotation. All stereoisomers expected for (*E,y*^{1}*,E,y*^{2}*,Z,y*^{3}*,Z,y*^{4})-isomers are mapped. See Figure S16 for the profiles involving (*E,y*^{1}*,E,y*^{2}*,Z,y*^{3}*,Z,y*^{4})-isomers.

The stereoisomers are mapped so that the adjacent isomers are interconvertible through bond rotations at a single biaryl linkage (hereafter denoted as single-linkage rotation).[48] The isomeric structures on the *x*-axis of the profiles cover all possible structures arising from the *R/S*-geometries.[49]

The two-stage transitions observed by VT NMR analysis showed the presence of low- and high-temperature isomerization processes. The low-temperature process was energetically similar to the isomerization of [10]CaNAP and was ascribed to the *E/Z* isomerization at the 3,3′-linkages of [8]CPhen$_{3,9}$. This process can be found as the vertical lines connecting neighboring stereoisomers in Figures 10 and S16. The high-temperature process was energetically similar to the isomerization of 9,9′-biphenanthrenyl and was ascribed to the *R/S* isomerization at the 9,9′-linkages of [8]CPhen$_{3,9}$. This process is represented by the horizontal lines connecting neighboring stereoisomers in Figures 10 and S16. Upon raising the temperature to surmount the energy barrier of $\Delta H^{\ddagger}$ = +25 kcal/mol, all stereoisomers of [8]CPhen$_{3,9}$ (Δ*E* < +25 kcal/mol) become accessible from the most stable enantiomers, i.e., (*E,S,E,S,E,S,E,S*)- and (*E,R,E,R,E,R,E,R*)-isomers, without consideration of concurrent rotations of multiple linkages. This possibility of stepwise single-linkage rotations for the isomerization is different from the requisite involvement of single-panel (double-linkage) rotations for the isomerization of belt-shaped nanohoops in the previous studies.[11,13,20] The panel rotations in the present profiles can be found in the diagonal lines connecting the neighboring stereoisomers. Provided that the energy barriers remained comparable to the +25-kcal/mol barrier of the single-linkage rotation, these processes could also be involved in the present system.[50,51]

CONCLUSIONS

We synthesized a cyclophenanthrenylene nanohoop ([8]-CPhen$_{3,9}$) possessing heterogeneous biaryl linkages. The *R/S* geometries at the 9,9′-linkages gave rise to the deviations of the nanohoop structures from the coplanar belt shapes and resulted in the cyclostereoisomerism that can be described by combinations of conventional *R/S* and *E/Z* descriptors. The non-belt-shaped structures gave rise to 51 stereoisomers with 31 diastereomers and 20 enantiomer pairs, and a pair of enantiomeric structures was found in the crystal. The studies on the dynamic isomerization processes revealed the presence of two-stage isomerizations that were respectively ascribed to the isomerization with the *E/Z* and *R/S* transitions. The *R/S* linkages at the 9,9′-connections were constrained at ambient temperature, and two enantiomeric isomers were separated. However, interestingly, the *E/Z* linkages at the 3,3′-connections were fluctuating at ambient temperature. Thus, two enantiomers are present as hoop-shaped structures of (*x,R,x,R,x,R,x,R*)- and (*x,S,x,S,x,S,x,S*)-isomers where linkages denoted as *x* are rapidly fluctuating structures between the *E* and *Z* geometries. The intrinsic axial chirality at the arylene linkages can give rise to the isolable stereoisomers of nanohoops but does not necessarily result in a persistent molecular shape. The experimental and theoretical studies of the energetics showed that all stereoisomers can be interconverted via stepwise single-linkage rotations, unlike the single-panel rotations required for the isomerization of belt-shaped cycloarylenes.[11,13,20] Through our studies on the stereoisomerism and molecular shapes, we may now categorize the nanohoop structures into three major types: (1) cylinder/tube/belt shapes, (2) fluctuating shapes, and (3) non-belt shapes.[10−12,19,20] We hope that the unique cyclostereoisomerism found in this study may deepen our understanding of nanohoop structural chemistry and may also facilitate the expansion of its scope to allied fields of chemistry.

ASSOCIATED CONTENT

Supporting Information

The Supporting Information is available free of charge on the ACS Publications website at DOI: 10.1021/acscentsci.6b00240.

Synthetic procedures and analytical data (PDF)

DOI: 10.1021/acscentsci.6b00240
ACS Cent. Sci. 2016, 2, 740−747

AUTHOR INFORMATION

Corresponding Author

*E-mail: isobe@m.tohoku.ac.jp. Tel: +81-(0)3-5841-4162.

Notes

The authors declare no competing financial interest.

ACKNOWLEDGMENTS

This work was partly supported by KAKENHI (24241036, 25102007, 16K04864). We thank KEK Photon Factory (No. 2015G097) for the use of the X-ray diffraction instruments.

REFERENCES

(1) Eliel, E. L.; Willen, S. H. *Stereochemistry of Organic Compounds*; Wiley: New York, 1994; Chapter 14.

(2) Quinkert, G.; Egert, E.; Griesinger, C. *Aspects of Organic Chemistry: Structure*; VCH: Basel, 1996; Chapters 2 and 10.

(3) Perlog, V.; Gerlach, H. Cycloenantiomerie und cyclodiastereomerie. 1. Mitteilung. *Helv. Chim. Acta* **1964**, *47* (8), 2288−2294.

(4) Lewis, S. E. Cycloparaphenylenes and related nanohoops. *Chem. Soc. Rev.* **2015**, *44*, 2221−2304.

(5) Segawa, Y.; Ito, H.; Itami, K. Structurally uniform and atomically precise carbon nanostructures. *Nat. Rev. Mater.* **2016**, *1*, 15002.

(6) Golder, M. R.; Jasti, R. Syntheses of the smallest carbon nanohoops and the emergence of unique physical phenomena. *Acc. Chem. Res.* **2015**, *48*, 557−566.

(7) Yamago, S.; Kayahara, E.; Iwamoto, T. Organoplatinum-mediated synthesis of cyclic π-conjugated molecules: Towards a new era of three-dimensional aromatic compounds. *Chem. Rec.* **2014**, *14*, 84−100.

(8) Komatsu, N. Stereochemistry of carbon nanotubes. *Jpn. J. Appl. Phys.* **2010**, *49*, 02BC01.

(9) Matsuno, T.; Naito, H.; Hitosugi, S.; Sato, S.; Kotani, M.; Isobe, H. Geometric measures of finite carbon nanotube molecules: A proposal for length index and filling indexes. *Pure Appl. Chem.* **2014**, *86*, 489−495.

(10) Hitosugi, S.; Nakanishi, W.; Yamasaki, T.; Isobe, H. Bottom-up synthesis of finite models of helical (*n*,*m*)-single-wall carbon nanotubes. *Nat. Commun.* **2011**, *2*, No. 492.

(11) Hitosugi, S.; Nakanishi, W.; Isobe, H. Atropisomerism in a belt-persistent nanohoop molecule: Rotational restriction forced by macrocyclic ring strain. *Chem. - Asian J.* **2012**, *7*, 1550−1552.

(12) Hitosugi, S.; Yamasaki, T.; Isobe, H. Bottom-up synthesis and thread-in-bead structures of finite (*n*,0)-zigzag single-wall carbon nanotubes. *J. Am. Chem. Soc.* **2012**, *134*, 12442−12445.

(13) Matsuno, T.; Kamata, S.; Hitosugi, S.; Isobe, H. Bottom-up synthesis and structures of π-lengthened tubular macrocycles. *Chem. Sci.* **2013**, *4*, 3179−3183.

(14) Conventional descriptors of planar chirality are not applicable to the belt-shaped sp^2-carbon networks because of the lack of pilot atoms (ref 1 10).

(15) European Mathematical Society, Encylclopedia of Mathematics, http://www.encyclopediaofmath.org/index.php?title=Cylinder&oldid=32421 (accessed Sept. 10, 2016).

(16) Wolfram, Wolfram MathWorld, http://mathworld.wolfram.com/Cylinder.html (accessed Sept. 10, 2016).

(17) Iijima, S. Helical microtubules of graphitic carbon. *Nature* **1991**, *354*, 56−58.

(18) Mathematically speaking, the term, "belt", is not a geometric description of the shapes. However, some chemists do not like the use of a correct, geometric term of "cylinder/tube" to describe our molecules, and we often use "belt" in place of "cylinder/tube". For further discussion on the lengths, see ref 9.

(19) Sun, Z.; Sarkar, P.; Suenaga, T.; Sato, S.; Isobe, H. Belt-shaped cyclonaphthylenes. *Angew. Chem., Int. Ed.* **2015**, *54*, 12800−12804.

(20) Sun, Z.; Suenaga, T.; Sarkar, P.; Sato, S.; Kotani, M.; Isobe, H. Stereoisomerism, crystal structures, and dynamics of belt-shaped cyclonaphthylenes. *Proc. Natl. Acad. Sci. U. S. A.* **2016**, *113*, 8109−8114.

(21) Nanohoops with 1,1′-binaphthyl linkages were reported, and [9]cyclo-1,4-naphthylene was reported to be "rigid" at ambient temperature with the presence of chirality proposed through theoretical investigations of two enantiomeric structures. See refs 22 and 23.

(22) Yagi, A.; Segawa, Y.; Itami, K. Synthesis and properties of [9]cyclo-1,4-naphthylene: A π-extended carbon nanoring. *J. Am. Chem. Soc.* **2012**, *134*, 2962−2965.

(23) Batson, J. M.; Swager, T. M. Torwards a perylene-containing nanohoop. *Synlett* **2013**, *24*, 2545−2549.

(24) Sarkar, P.; Dechambenoit, P.; Durola, F.; Bock, H. Synthesis of carboxy-functionalized polycyclic arenes by oxidative cyclizations of 2,3-diarylacrylates. *Asian J. Org. Chem.* **2012**, *1*, 366−376.

(25) Wood, C. S.; Mallory, F. B. Photochemistry of stilbenes. IV. The preparation of substituted phenanthrenes. *J. Org. Chem.* **1964**, *29*, 3373−3377.

(26) Leroux, F. R.; Simon, R.; Nicod, N. A highly efficient low temperature modification of the classical Ullmann reaction. *Lett. Org. Chem.* **2006**, *3*, 948−954.

(27) Ishiyama, T.; Murata, M.; Miyaura, N. Palladium(0)-catalyzed cross-coupling reaction of alkoxydiboron with haloarenes: A direct procedure for arylboronic esters. *J. Org. Chem.* **1995**, *60*, 7508−7510.

(28) Adams, R.; Yuan, H. C. The stereochemistry of diphenyls and analogous compounds. *Chem. Rev.* **1933**, *12*, 261−338.

(29) Kuhn, R.; Albrecht, O. Racemisierungsversuche an optisch aktiven diphensäuren. (Zur stereochemie aromatischer verbindungen, V). *J. Liebigs Ann. Chem.* **1927**, *458*, 221−229.

(30) Kuhn, R.; Albrecht, O. Über die racemisierung optisch aktiver diphensäuren und über die schwingungen der benzolkerne im diphenylsystem. (Zur stereochemie aromatischer verbindungen, IV). *J. Liebigs Ann. Chem.* **1927**, *455*, 272−299.

(31) The energy barriers of [*n*]CaNAP were also located at the *E*/*Z* transitions (ref 20).

(32) Racemization energy barriers from the experiments indicated that the PM6 scan analysis underestimated the energy barriers for the biaryl rotations.

(33) Anet, F. A. L.; Basus, V. J. Limiting equations for exchange broadening in two-site NMR systems with very unequal populations. *J. Magn. Reson.* **1978**, *32*, 339−343.

(34) Okazawa, N.; Sorensen, T. S. The line-shape analysis of nuclear magnetic resonance peaks broadened by the presence of a 'hidden' exchange partner. *Can. J. Chem.* **1978**, *56*, 2737−2742.

(35) Katritzky, A. R.; Patel, R. C.; Read, D. M. The synthesis and conformational analysis of perhydro-1,2,4-triazines and perhydro-1,3,4-thiadiazines and a note on. *Tetrahedron Lett.* **1977**, *18*, 3803−3806.

(36) We noticed that oxidation of [8]$CPhen_{3,9}$ proceeded under the current HPLC conditions to afford minor peaks in front of the major peaks.

(37) Bauernschmitt, R.; Ahlrichs, R. Treatment of electronic excitations within the adiabatic approximation of time dependent density functional theory. *Chem. Phys. Lett.* **1996**, *256*, 454−464.

(38) This assignment of the absolute configuration in ref 10 was unequivocally confirmed by crystallographic analysis. See ref 39.

(39) Sato, S.; Yamasaki, T.; Isobe, H. Solid-state structures of peapod bearings composed of finite single-wall carbon nanotube and fullerene molecules. *Proc. Natl. Acad. Sci. U. S. A.* **2014**, *111*, 8374−8379.

(40) At ambient temperature, rapid *E*/*Z* isomerization of [8]$CPhen_{3,9}$ at 3,3′-linkages can readily proceed (see below), and the structure is fluctuating among (*x*,*R*,*x*,*R*,*x*,*R*,*x*,*R*)/(*x*,*S*,*x*,*S*,*x*,*S*,*x*,*S*)-diastereomers with *x* being *E* or *Z* geometries. As a result of this *E*/*Z* isomerization, the conjugation at the 3,3′-linkages is not persistently present.

(41) For this assignment, the theoretical signals are red-shifted by ca. 25 nm.

(42) The enantiomers of **4** were separated by HPLC using Daicel Chiralpack AD column and designated by using signs of the CD signals at 300 nm.

(43) As reported in the literature (refs 28−30), the half-life was obtained by $t_{1/2} = k^{-1}\cdot\ln 2$.

DOI: 10.1021/acscentsci.6b00240
ACS Cent. Sci. 2016, 2, 740−747

(44) Cooke, A. S.; Harris, M. M. Ground-state strain and other factors influencing optical stability in the 1,1′-binaphthyl series. *J. Chem. Soc.* **1963**, *0*, 2365−2373.
(45) The difference of entropy terms for **4** and [8]CPhen$_{3,9}$ should be ascribed to the presence of *E*/*Z* fluctuations in the isomerization of [8]CPhen$_{3,9}$.
(46) Nakanishi, W.; Shimada, Y.; Isobe, H. Structural fluctuation of disilanyl double-pillared bisheteroarenes. *Chem. - Asian J.* **2013**, *8*, 1177−1181.
(47) Fujino, T.; Okada, K.; Isobe, H. Conformational restriction of cyclic dinucleotides with triazole-linked cyclophane analogues. *Tetrahedron Lett.* **2014**, *55*, 2659−2661.
(48) There appears two paths for the isomerization of (E,y^1,E,y^2,E,y^3,E,y^4)-isomer to (Z,y^1,Z,y^2,Z,y^3,Z,y^4)-isomer under the condition of single-linkage rotations. Figure 9 shows the path via (E,y^1,Z,y^2,E,y^3,Z,y^4), and Figure S16 shows the path via (E,y^1,E,y^2,Z,y^3,Z,y^4). Two profiles were necessary to cover the 51 steroisomers in total.
(49) Although multiple possible orders of isomers are present for the single-linkage rotations, the profiles were created by using one representative path for the racemization of [8]CPhen$_{3,9}$ via single-linkage rotations.
(50) Sarkar, P.; Sato, S.; Kamata, S.; Matsuno, T.; Isobe, H. Synthesis and dynamic structures of a hybrid nanohoop molecule composed of anthanthrenylene and phenylene panels. *Chem. Lett.* **2015**, *44*, 1581−1583.
(51) There are different types of panel rotations appeared in the diagonal lines. For instance, (E,S,E,S,E,S,$\underline{E}$,$\underline{S}$)- and (E,S,E,S,E,S,$\underline{Z}$,$\underline{R}$)-isomers are interconverted by a single-panel rotation, and (E,$\underline{R}$,Z,R,$\underline{E}$,S,Z,R)- and (E,$\underline{S}$,Z,R,$\underline{Z}$,S,Z,R)-isomers are interconverted by a correlated rotation of multiple panels (ref 50).

DOI: 10.1021/acscentsci.6b00240
ACS Cent. Sci. 2016, 2, 740−747